Experimental visualization of aluminum ignition and burning close to a solid propellant burning surface

Thomas Geoffrey Decker, Robin William Devillers, Stany Gallier

Experimental visualization of aluminum ignition and burning close to a solid propellant burning surface

Thomas Geoffrey Decker*[1], Robin William Devillers[1], and Stany Gallier[2]

[1]DMPE, ONERA, Université Paris Saclay, Palaiseau, F-91123, France
[2]ArianeGroup SAS, Le Bouchet Research Center, 91710 Vert le Petit, France

Abstract

Visible images of burning solid propellants loaded with aluminum particles are presented. The images are recorded at high acquisition frame rate (up to $33kHz$) with excellent sharpness, enabling the study of aluminum ignition and combustion close to the propellant burning surface. The article focuses on two aspects: the aluminum aggregate ignition and the alumina breaking and migration on the aggregate surface. The article presents new ways of studying aluminum agglomeration and combustion by applying image processing algorithms on state-of-the-art image series.

1 Introduction

Solid Rocket Motors (SRM) are widely used in military and civilian applications. They are highly reliable, require little maintenance, and are readily available even when stored for a long time. A solid propellant is a solid material used to generate thrust by its combustion. It is composed of a fuel binder and oxidizing particles. Metal particles, usually aluminum, are added to increase the propulsion performances with additional combustion heat release. While the fuel and the oxidizer burn at the propellant surface, the aluminum particles burn in the gas flow produced by the fuel/oxidizer combustion. The aluminum particles are subject to complex phenomena prior to their combustion in the gas flow [1, 2]. They follow an accumulation-aggregation-agglomeration mechanism [3, 4]. The particles accumulate in the solid propellant pockets [5], they aggregate while being attached to the burning surface and finally agglomerate when they ignite on the burning surface or in the gas flow. The aluminum particles are referred as aggregates (on the burning surface, with a coral-like shape, eventually morphing into a spherical one), and agglomerates (in the gas flow, with a spherical shape). The resulting droplets can reach hundreds of micrometers in diameter [6], while the virgin particle size is usually between 5 and $50\mu m$. An oxide (alumina) cap is attached to the burning aluminum droplet. The droplet combustion produces heat as well as alumina, with some parts being evacuated in the gas flow as smoke while another portion increases the size of the oxide cap.

The inert alumina droplets produced during the aluminum combustion influences the stability and the performances of the SRM, depending on their size [7, 8]. The particles often follow a trimodal distribution [9] when captured with collection techniques ([2, 10, 11]). The lower and higher modes of the size distribution are respectively attributed first to alumina smokes and second to the aluminum agglomerates and coarse oxide, but the intermediate mode ($4-8\mu m$) is not fully understood [9], and doubts remain about the production of those alumina droplets. The alumina production mechanism during the aluminum droplet combustion is considered in many studies [12, 13]. But its production close to the surface when the aluminum is still attached to the propellant has never been studied to the authors' knowledge. No model for oxide-cap formation during the aggregation-agglomeration mechanism has been published. This formation is crucial because the alumina migration to form an oxide cap influences the aluminum ignition on the burning surface while the size of the resulting oxide cap influences the aluminum combustion along the droplet lifetime [12, 14, 15].

Two phenomena associated with the alumina production and oxide cap formation on the burning surface are studied with image processing: the aluminum aggregate ignition and the alumina layer breaking and migration. This study shows new ways of studying physical phenomena associated with aluminum agglomeration and combustion in solid propellants.

2 Experimental setup and data

Shadowgraphy was used to visualize accurate details above the solid propellant surface during combustion [16]. Here a similar optical set-up was used without back illumination to improve the contrast between aluminum and alumina. A high-speed camera acquires frames to target physical phenomena on the solid propellant burning surface. The acquisition rate was adjusted up to $33kHz$, and the recorded images size depends on the frame rate. The spatial resolution is about $3.2\mu m/px$.

Two solid propellants are studied ($P1$ and $P2$). Their compositions are similar. Both include a trimodal repartition of Ammonium Perchlorate (AP) particles, a hydroxyl-terminated polybutadiene (HTPB) binder and approximately 20% of aluminum particles. They only differ in the initial size of the aluminum particles. The $P1$ initial aluminum particles size is approximately $30\mu m$ while the $P2$ is approximately $15\mu m$. In order to capture the aluminum particles or agglomerates as clearly as possible, propellants are beveled. The cam-

*Corresponding author: thomas.decker@onera.fr

era views the propellant slightly from the top with an angle around 45°. Heated aluminum and alumina are clearly visible because of their incandescence.

The $P1$ propellant is studied at two initial pressures, 5 and 10 *bar*. It is recorded at $14kHz$ in order to capture the aluminum ignition of the aggregates. The $P2$ propellant is studied at one initial pressure, 5 *bar*. It is recorded at $33kHz$ in order to capture the aluminum breaking and migration. Image examples are presented in figures 1, 2, and 3.

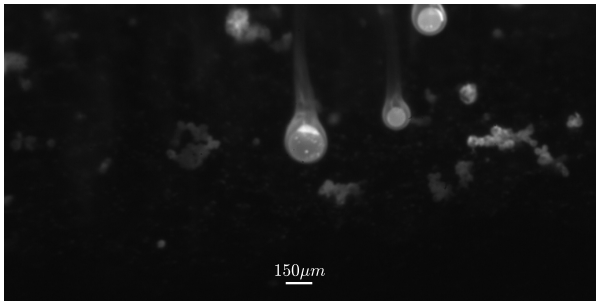

Figure 1: Image of the $P1$ propellant at the initial pressure of 5 *bar*. Agglomerates are visible in the gas flow, and aggregates (igniting or not) on the burning surface.

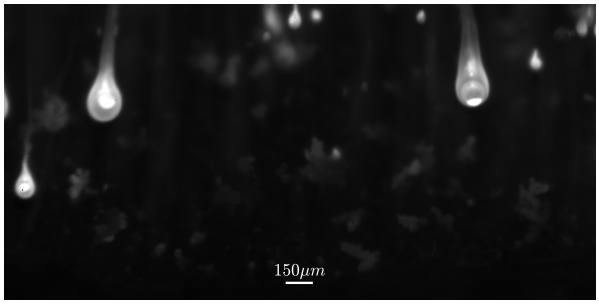

Figure 2: Image of the $P1$ propellant at the initial pressure of 10 *bar*.

The surface on the image of the $P1$ propellant at 10 *bar* is brighter than at 5 *bar* (the experimental setup is kept identical). The solid propellant flames are closer to the surface with increasing pressure. The aluminum close to the surface is therefore hotter, i.e. brighter.

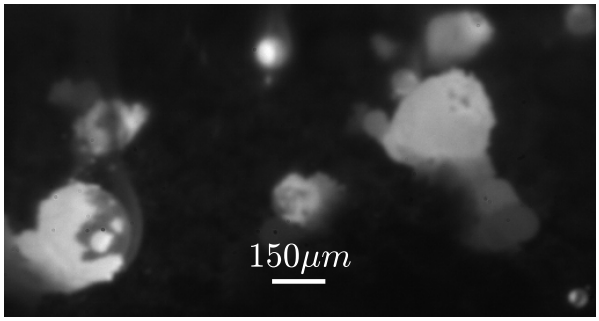

Figure 3: Image of the $P2$ propellant at the initial pressure of 5 *bar*. Aggregates transforming into agglomerates are visible on the left and in the middle.

3 Image processing

3.1 Aggregates detection

The first studied phenomenon is the aluminum aggregates ignition on the burning surface of the propellant. The objective is to automatically detect and track the aluminum aggregates and agglomerates on the propellant surface and in the gas flow. The number of captured images for the $P1$ propellant at the initial pressures of 5 and 10 *bar* being approximately 2000 and 2500, automatic algorithms are needed. The following processing steps were used:

Step 1 - Top-hat filtering

The Top-hat transform [17] extracts elements from given images. The transform depends on a structuring element, usually a disk. The bright objects with much smaller sizes are considered as part of the background. Therefore, only the aggregates with sufficient sizes can be easily detected.

Step 2 - Thresholding

A simple thresholding of the resulting image enables the detection of the aggregates and agglomerates on the burning surface. The threshold choice is a compromise in order to avoid merging separate aggregates into a single detected object.

Figure 5 shows steps 1 and 2 for the $P1$ propellant at 5 *bar*, compared to the color scale limited original image shown in figure 4.

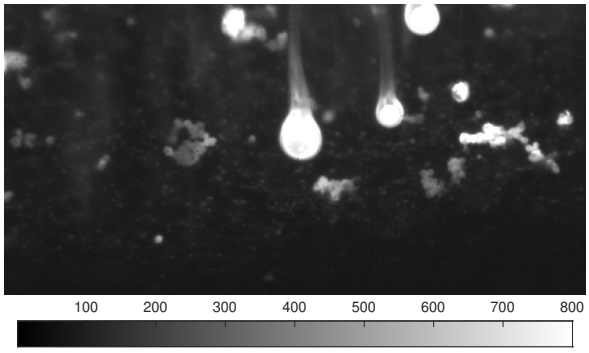

Figure 4: Image of the $P1$ propellant at the initial pressure of 5 *bar* with a limited color-scale.

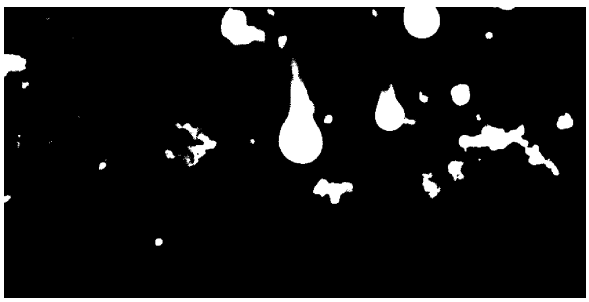

Figure 5: Thresholding following the Top-hat transform application on the image of the $P1$ propellant at the initial pressure of 5 *bar*.

Steps 3 and 4 - Detection and tracking

The resulting thresholded image is binary. The aggregates and agglomerates are easily detected. Metrics are automatically calculated, such as the area, the circularity, the mean and the maximum intensity.

The resulting detections are tracked on successive images to analyze the behavior of aggregates on the

solid propellant surface. Thanks to the significant frame rate, a simple Intersect-Over-Union (IOU) threshold is employed. Two tracked aggregates at 5 and 10 *bar* can be visualized in figures 6a and 6c).

3.2 Alumina detection

The second studied phenomenon is part of the aggregate ignition, it is the alumina breaking and migration. The objective is to detect and track alumina on the surface of aluminum aggregates. In order to study the phenomenon, the frame rate is much higher, $33kHz$. We focus here on one sequence of approximately 300 frames where the alumina encapsulating an aggregate breaks up and migrates.

A Top-hat transform is applied, followed by a thresholding. An example is shown in figure 7 for propellant $P2$ at 5 *bar* with (a) Top-Hat transform and (b) Threshold image. Figure 7 zooms on a igniting aggregate on the propellant surface.

The detection algorithm can segment the main alumina surface surrounding the aluminum collapsing into a lobe (on the left-hand side) but also isolated alumina portions moving on the aluminum surface (on the right-hand side) that will eventually reach the forming oxide cap.

Several metrics are automatically calculated, such as the area, the circularity, the mean and the maximum intensity. The main alumina surface is easily tracked over time, as the largest detection. We follow other alumina detections with the IOU calculation. Here, the minimum IOU is fixed very low because of the rapid motion of the alumina zones compared to their size. Figure 8a shows the evolution of the main alumina layer that initially surrounds the whole liquid aluminum, and figure 9a shows successive positions of a single alumina portion.

4 Results and discussion

4.1 Aggregates ignition

Here are comments on the aggregate ignition on the surface by analyzing two aggregates tracked other time (figures 6a and 6c). The metrics are plotted in figure 6b.

The growth of the detected areas of the two aggregates on the burning surface (see images 1 to 4 from figure 6a and images 1 to 3 from figure 6c) can be observed with the area. Only fragments of the aggregated are detected for the first detection because the overall aggregate is not bright enough at this early heating stage. The detections grow with time as more and more portions of the aggregates become sufficiently bright.

The increase in temperature of a tracked aggregate is not only synonymous with an increase of the detected area but also a steady increase in the mean intensity (see images 1 to 4 from 6a and 1 to 3 from figure 6c). The mean intensity slowly increases from 2.5 to 4.0ms for the aggregate at 5 *bar* (blue plot) while the intensity increase happens from 1.1 to 2.0ms at 10 *bar* (red plot). The intensity spike happening around 0.3ms in the red plot corresponds to a burning droplet passing nearby in its upwards movement.

When the aggregates are ignited and transformed into agglomerates, they establish a diffusion flame with the surrounding gas (see image 6 from 6a and image 5 from figure 6c). The diffusion flame establishment corresponds to an increase in area, an increase in mean intensity and a decrease in circularity. Simultaneously, the newly formed agglomerates leave the surface and move in the gas flow. The movement in the gas flow is visible with the vertical velocity increase starting at 5ms at 5 *bar* and 4.2ms at 10 *bar*.

The metrics are calculated for each tracked aggregate on the burning surface detected for at least five frames. 786 aggregates were tracked at 5 *bar* and 1259 at 10 *bar*. Two estimates are calculated for each tracks

- The track duration time gives the estimate of the ignition time τ
- A mean intensity *Imean* is calculated over the complete track

Distributions for the two estimated are presented in figures 10a and 10b. To avoid visualizing the threshold effect with a spike of distribution on the lowest values, the distribution of the ignition time is presented as a cumulative. The ignition time τ is globally lower at 5 *bar* than at 10 *bar*. The aggregates ignition is faster with increasing pressure. A shorter ignition delay leads to less agglomeration. It is consistent with the physics of aluminum agglomeration in solid propellants, agglomerates are smaller with increasing pressure [18, 19].

The mean intensity $\overline{I_{mean}}$ is globally increasing with increasing pressure. Propellant flames get closer to the burning surface with increasing pressure, leading to a more efficient aggregate heating (i.e. brighter detections).

Overall, tracking aluminum aggregates on the burning surface enables the study of physical phenomena associated to aluminum agglomeration, ignition, and combustion on the solid propellant burning surface. It helps understand the importance of the aggregates' temperature on its ignition. The study of the detected area shows that the aggregates are not homogeneous in temperature. Data also show the importance of temperature in the aggregates ignition. With increasing pressure, the solid propellant flames are closer to the burning surface, the aggregates are hotter, resulting in a decreasing ignition time.

A more quantitative study is required to compare the ignition time of the aggregates to their residence time on the propellant surfaces. Models would have to include ignition delay if its time range is comparable to the residence time on the burning surface. A more detailed study could put into equation the ignition time depending on physical parameters such as pressure, the propellant constitution or the aggregate size.

4.2 Alumina breaking and migration

The second focus is on the alumina breaking and migration of an aluminum aggregate attached to the solid propellant burning surface. The alumina breaking and migration exposes the liquid aluminum to the surrounding oxidizing gas. Therefore, the liquid aluminum starts to burn and establishes a diffusion flame (see images 4

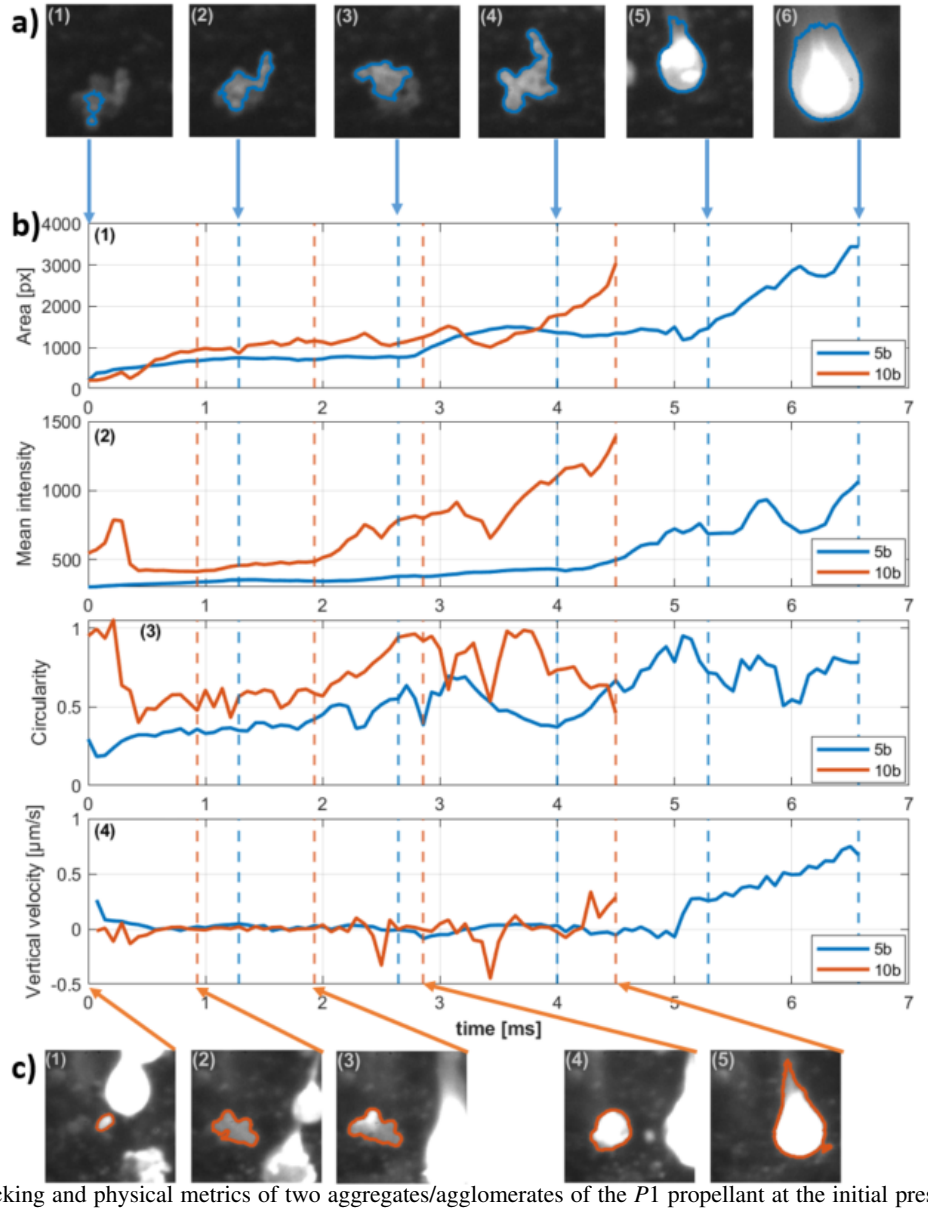

Figure 6: Tracking and physical metrics of two aggregates/agglomerates of the $P1$ propellant at the initial pressures of 5 and 10 *bar*.

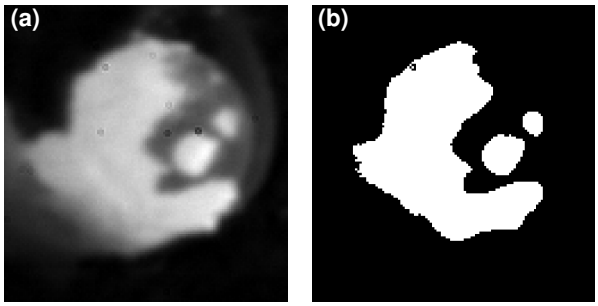

Figure 7: (a) Top-hat transform application on the zoomed image on an aggregate of the $P2$ propellant at the initial pressure of 5 *bar*, (b) Thresholding of the resulting image

to 6 from figure 8a). We focus on two tracks, the main alumina surface that initially surrounds the whole aluminum aggregate and an isolated alumina portion moving rapidly on the liquid alumina surface. Metrics associated with the two tracks are presented in figures 8b and 9b.

The main alumina surface follows a first period of $\sim 7ms$ where it keeps a circular shape but seems to have a variable temperature (i.e. a variable mean intensity in figure 8b). The exothermic production of alumina is a possible explanation of the increased temperature (i.e. an increased mean intensity in figure 8b between 2.5 and $5ms$) prior to the alumina breaking. Price et al. [1] demonstrated that the encapsulating alumina cracks due to the expanding liquid aluminum. The liquid aluminum finds itself partially exposed, resulting in the production of additional alumina.

Then, the alumina surface breaks up on the top of the aggregate (where it is supposed to be hotter), a local temperature increase occurs due to the released liquid aluminum combustion, and the circular alumina surface retracts. The alumina break up happens at $\sim 7ms$. The alumina may move on the aluminum surface as small portions. The phenomenon is very rapid, as shown in

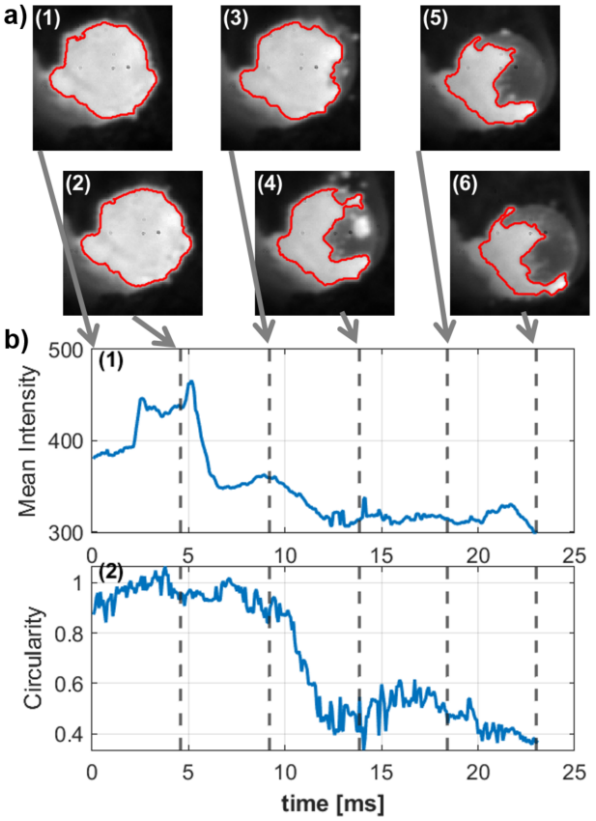

Figure 8: Tracking and physical metrics of the main alumina surface of an aggregate of the *P*2 propellant at the initial pressure of 5 *bar* (thumbnails zoomed).

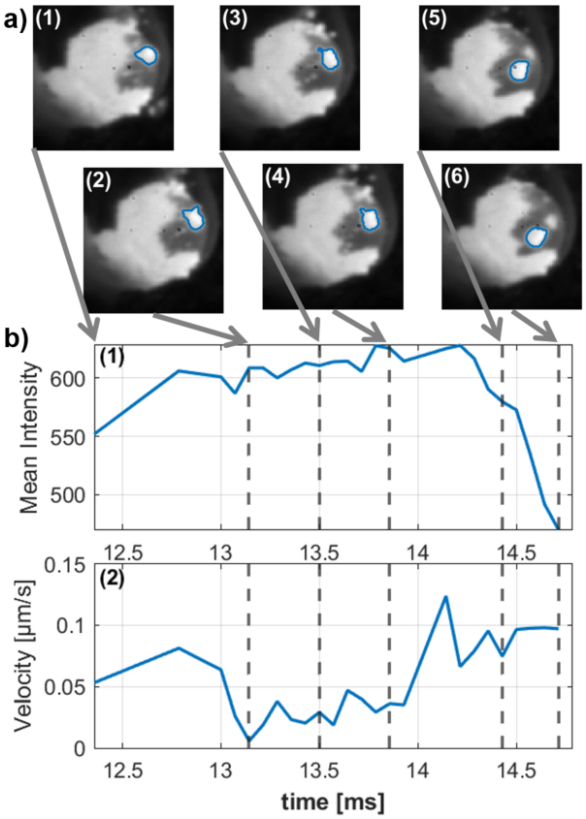

Figure 9: Tracking and physical metrics of a moving alumina portion of an aggregate of the *P*2 propellant at the initial pressure of 5 *bar* (thumbnails zoomed).

figure 9b (the total duration of the alumina movement being only a few *ms*). The alumina may also be ejected as small drops (see images 3 and 4 from figure 9a).

The small tracked alumina portion also has a variable temperature (i. e. a variable mean intensity) as shown in figure 9b. It seems that its temperature decreases when it is moving from the top of the liquid aluminum to the main alumina surface, meaning that the aluminum aggregate has a vertical temperature gradient. It confirms the analysis in the previous section that the aggregate temperature is not homogeneous.

The movement of alumina on the liquid aluminum stops at $\sim 14ms$. The reason attributed here is that the aluminum of this aggregate does not produce enough heat. The alumina produced on the liquid aluminum surface tempers the combustion and slowly passivates the aggregate. It is visually observed that some igniting aggregates can be passivated. Another ignition needs to occur to finalize the transition from aggregate to agglomerate.

Overall, significant alumina production occurs on the liquid aluminum surface, during the residence of the aluminum aggregate on the solid propellant burning surface. The produced alumina then migrates into the oxide cap. Therefore, a portion of the final residue is produced when the aluminum aggregate is attached to the propellant burning surface. This study shows the importance of physical phenomena associated to aluminum on a solid propellant surface, influencing the size of the resulting alumina cap, and affecting the stability of a SRM.

5 Conclusion

Visible images of burning solid propellants loaded with aluminum particles were presented. Physical phenomena associated with alumina production were studied thanks to high-speed recording, excellent spatial resolution, good image clearness, and new algorithms using a Top-hat transform.

Different stages of the aggregated aluminum ignition were shown at two initial pressures, 5 and 10 *bar*. Aggregate temperature increases before it ignites and transforms into a spherical agglomerate. It was found that the ignition time decreases with increasing pressure. The mean intensity of the aggregates increases with increasing pressure, meaning that the aggregates are hotter on the burning surface. Increased pressure leads to closer solid propellant flames to the burning surface and the aggregates.

The alumina breaking and migration were observed thanks to a test at a very high frame rate of $33kHz$. An alumina portion was even tracked on a liquid aluminum droplet. Small aluminum/alumina drops were observed being ejected in the gas flow during the surrounding alumina surface migration. A significant production of alumina occurs on the liquid aluminum surface. To the authors' knowledge, those phenomena were never studied in the literature. This study shows the importance of the

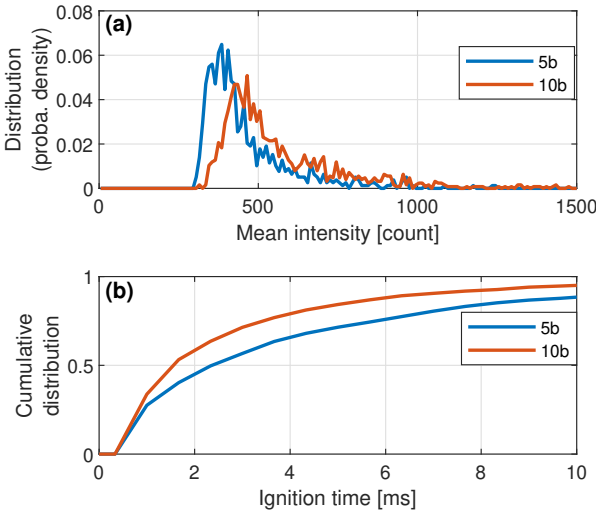

Figure 10: Distributions for the tracked aggregates at 5 and 10 *bar*. (a) Mean Intensity distribution, (b) Ignition time cumulative distribution

phenomena highlighted in the domain of SRM stability.

The study showed the importance of the aggregates' temperature during their ignition. The study also showed that aggregates ignite with a delay, depending on pressure. With refined data analysis, quantitative data about the temperature gradient depending on pressure or aggregate size could be calculated. Its influence on the aluminum aggregate ignition delay could also be investigated. Quantitative data on the aggregate temperature gradient and its ignition delay will be useful for future aluminum agglomeration models.

6 Acknowledgment

Thomas Decker's PhD is financed by ONERA and ArianeGroup. S. G. thanks DGA (French Procurement Agency) for funding.

References

[1] E. W. Price and R. K. Sigman, Combustion of aluminized solid propellants, *Progress in Astronautics and Aeronautics* **185**, 663 (2000).

[2] V. A. Babuk, V. A. Vasilyev, and V. V. Sviridov, Formation of condensed combustion products at the burning surface of solid rocket propellant, *Progress in Astronautics and Aeronautics* **185**, 749 (2000).

[3] F. Maggi, S. Dossi, and L. T. DeLuca, Combustion of metal agglomerates in a solid rocket core flow, *Acta Astronautica* **92**, 163 (2013).

[4] W. Ao, X. Liu, H. Rezaiguia, H. Liu, Z. Wang, and P. Liu, Aluminum agglomeration involving the second mergence of agglomerates on the solid propellants burning surface: experiments and modeling, *Acta Astronautica* **136**, 219 (2017).

[5] N. S. Cohen, A pocket model for aluminum agglomeration in composite propellants, *AIAA J.* **21**, 720 (1983).

[6] V. Babuk, I. Dolotkazin, A. Gamsov, A. Glebov, L. T. DeLuca, and L. Galfetti, Nanoaluminum as a solid propellant fuel, *Journal of Propulsion and Power* **25**, 482 (2009).

[7] M. Salita, Deficiencies and requirements in modeling of slag generation in solid rocket motors, *J. Prop. Power* **11**, 10 (1995).

[8] Z. Li, N. Wang, B. Shi, S. Li, and R. Yang, Effects of particle size on two-phase flow loss in aluminized solid rocket motors, *Acta Astronautica* **159**, 33 (2019).

[9] V. E. Zarko and O. G. Glotov, Formation of al oxide particles in combustion of aluminized condensed systems, *Science and Technology of Energetic Materials* **74**, 139 (2013).

[10] K. Jayaraman, S. Chakravarthy, and R. Sarathi, Quench collection of nano-aluminium agglomerates from combustion of sandwiches and propellants, *Proceedings of the Combustion Institute* **33**, 1941 (2011).

[11] H. Liu, W. Ao, Q. Hu, P. Liu, S. Hu, L. Liu, and Y. Wang, Effect of rdx content on the agglomeration, combustion and condensed combustion products of an aluminized htpb propellant, *Acta Astronautica* **170**, 198 (2020).

[12] M. W. Beckstead, Tech. Rep., Brigham Young Univ Provo Ut (2004).

[13] V. Karasev, A. Onischuk, O. Glotov, A. Baklanov, A. Maryasov, V. Zarko, V. Panfilov, A. Levykin, and K. Sabelfeld, Formation of charged aggregates of al2o3 nanoparticles by combustion of aluminum droplets in air, *Combustion and Flame* **138**, 40 (2004).

[14] M. W. Beckstead, Correlating aluminum burning times, *Combustion, Explosion and Shock Waves* **41**, 533 (2005).

[15] M. K. King, Aluminum combustion in a solid rocket motor environment, *Proceedings of the combustion institute* **32**, 2107 (2009).

[16] R. W. Devillers, G. Le Besnerais, M. Nugue, and N. Cesco, in *7th European Conference for Aeronautics and Space Sciences, Milan (Italy)* (2017).

[17] E. R. Dougherty, in *SPIE* (Optical Engineering Press, 1992).

[18] P. F. Pokhil, A. F. Belyaev, Y. V. Frolov, V. S. Logachev, and A. I. Korotkov, Combustion of metal powders in active media, *Defense Technical Information Center, Technical Report AD0769576* (1972).

[19] J. K. Sambamurthi, E. W. Price, and R. K. Sigman, Aluminum agglomeration in solid-propellant combustion, *AIAA J.* **22**, 1132 (1984).